

The Asian Dust Aerosol Model 2 (ADAM2) with the use of Normalized Difference Vegetation Index (NDVI) obtained from the Spot4/vegetation data

Soon-Ung Park · Anna Choe · Eun-Hee Lee ·
Moon-Soo Park · Xingzhuo Song

Received: 27 September 2008 / Accepted: 12 May 2009 / Published online: 7 February 2010
© Springer-Verlag 2010

Abstract The operational Asian Dust Aerosol Model (ADAM)1 in Korea Meteorological Administration has been modified to the ADAM2 model to be used as an operational forecasting model all year round not only in Korea but also in the whole Asian domain (70–160°E and 5–60°N) using the routinely available World Meteorological Organization (WMO) surface reporting data and the Spot/vegetation Normalized Difference Vegetation Index (NDVI) data for the period of 9 years from 1998 to 2006. The 3-hourly reporting WMO surface data in the Asian domain have been used to re-delineate the Asian dust source region and to determine the temporal variation of the threshold wind speed for the dust rise. The dust emission reduction factor due to vegetation in different surface soil-type regions (Gobi, sand, loess, and mixed soil) has been determined with the use of NDVI data. It is found that the threshold wind speed for the dust rise varies significantly with time (minimum in summer and maximum in winter) and surface soil types with the highest threshold wind speed of 8.0 ms^{-1} in the Gobi region and the lowest value of 6.0 ms^{-1} in the loess region. The statistical analysis of the

spot/vegetation NDVI data enables to determine the emission reduction factor due to vegetation with the free NDVI value that is the NDVI value without the effect of vegetation and the upper limit value of NDVI for the dust rise in different soil-type regions. The modified ADAM2 model has been implemented to simulate two Asian dust events observed in Korea for the periods from 31 March to 2 April 2007 (a spring dust event) and from 29 to 31 December 2007 (a winter dust event) when the observed PM_{10} concentration at some monitoring sites in the source region exceeds $9,000 \mu\text{g m}^{-3}$. It is found that ADAM2 model successfully simulates the observed high dust concentrations of more than $8,000 \mu\text{g m}^{-3}$ in the dust source region and $600 \mu\text{g m}^{-3}$ in the downstream region of Korea. This suggests that ADAM2 has a great potential for the use of an operational Asian dust forecast model in the Asian domain.

1 Introduction

Asian dust, called “Hwangsa” in Korea and “Kosa” in Japan, is a typical example of mineral aerosol frequently originating in the Gobi Desert, sand desert, Loess Plateau, and barren mixed soil in Northern China and Mongolia during the spring season and occasionally during the winter season. Dust storms occurring in East Asian desert regions tend to cause major aerosol events well beyond the Asian continent (Husar et al. 2001). The occurrences of strong dust storms are often associated with catastrophic consequences to humans and their environment. Indeed, very severe dust storms were observed in Korea on 21–23 March and 7–9 April 2002 (Park and Lee 2004). During these periods, the observed PM_{10} concentrations were over $1,500 \mu\text{g m}^{-3}$ at most monitoring sites in South Korea, causing natural

S.-U. Park (✉) · A. Choe · M.-S. Park
Center for Atmospheric and Environmental Modeling,
Seoul National University Research Park,
Rm. 515, San 4-2, Bongcheon-dong, Gwanak-gu,
Seoul, South Korea 151-919
e-mail: supark@snu.ac.kr

E.-H. Lee
Seoul National University,
Seoul 151-747, South Korea

X. Song
Peking University,
Beijing 100871, China

disasters, including temporal closing of most of airports and elementary schools in Korea (Park and Lee 2004).

In 2002, the Asian Dust Aerosol Model (ADAM) has been developed on the basis of a statistical method of the dust emission conditions using the World Meteorological Organization's 3-hourly synoptic reporting data for 7 years from 1996-2002 in the source region (Park and In 2003; In and Park 2003). The ADAM model successfully simulated the temporal and spatial distribution of dust concentration and the starting and ending times of Asian dust events observed in Korea during 21-22 March and 7-9 April 2002 (Park and In 2003; Park and Lee 2004). However, the model tended to overestimate the dust concentration in the late spring of May that might be caused by not taking into account the growth of vegetation in the Asian dust source regions.

Lee and Park (2005) have developed the ADAM1 model (they called the model as ADAM2; hereafter, it will be called as ADAM1 for a consistent sequence) on the basis of the ADAM model by taking into account the observed monitoring tower data at Duolun in Inner Mongolia and the changes of land use types in the source regions. The modification has been done by comparing modeled and monitored meteorological parameters including the relative humidity, soil surface temperature, surface friction velocity, and surface vegetation conditions. This model has been able to simulate quite reasonably the Asian dust events observed in Korea since 2003 (Lee and Park 2005). However, the vegetation distributions used in the model in the dust source regions are restricted only to the spring time when the dust occurrence frequency is highest so that the ADAM1 model cannot be used for estimating dust concentration all year round.

Both ADAM and ADAM1 use the total dust emission flux parameterized for Saharan dust outbreaks (Westphal et al. 1987; Gillette 1981) where the sand soil predominates. However, the Asian dust source regions are composed of Gobi, sand, loess, and mixed soils (Park and In 2003; Park and Lee 2004; In and Park 2002; 2003) so one type of soil may not be relevant in estimating the dust emission amount. To take into account different soil types for the parameterization of the dust emission flux from different soil types of the surface, Park and Lee (2005) have developed a parameterization of the total dust emission flux from different source regions using the saltation fluxes (Marticorena and Bergametti 1995) with the observed clay content in each soil type. The newly parameterized total dust emission flux, what they called, "the modified ADAM model" has been employed for the simulation of a dust event observed in Korea from 20-22 April 2005. The model was capable of simulating the starting and ending times of the dust event and the maximum dust concen-

trations observed in South Korea slightly better than those results of the ADAM1 model.

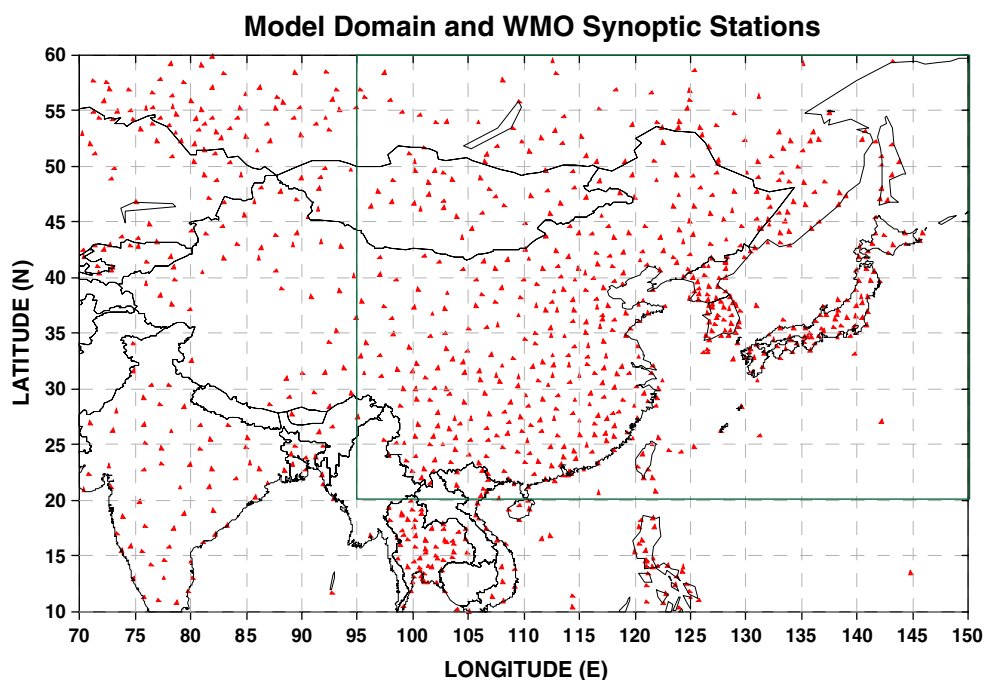
ADAM1 as an operational model to forecast dust events in Korea Meteorological Administration (KMA) since 2003 has been used mainly to forecast dust events over the Korean Peninsula during the spring season when the frequency of the observed Asian dust events in Korea is highest. The model, therefore, uses a rather small domain (60-20°N and 95-150°E; Fig. 1) with fixed land use types. However, many Asian countries that do not have their own dust prediction models want to use the results of the ADAM model. This calls for an expansion of the model domain (Fig. 1) and for a model that can be run the whole year round since Asian dusts occur all year round somewhere in Asian dust source regions. Therefore, some parameters in the ADAM model should be changed to yield more accurate results in predicting Asian dust events in Asia.

One of the most important controlling factors for dust emission and intensity is the reduction of vegetation in the source region over time. However, all the ADAM models mentioned above use time-independent emission reduction factors in the source regions, estimated by the United States Geological Survey (USGS) land-use types even though emission reduction factors can be changed along with changes in the surface properties, caused by the growth of grasses and trees and the expansion of cultivated land in the source regions.

Recently, the remote sensing has been applied to monitor the desertification and to access the amount of the vegetation in arid and semi-arid regions (Huang and Siebert 2006; Tucker et al. 1991). Satellite vegetation monitoring using red and near-infrared channels has been one of the most widely used indices of change of vegetation coverage (Telesca and Lasaponara 2006). The Normalized Difference Vegetation Index (NDVI) is known to correlate highly with green biomass and the leaf area index (Wu and Liu 2000; Lu et al. 2005; Wang et al. 2005). Also, the number of dust storm days is known to have a correlation with NDVI in spring, especially in Central and East Inner Mongolia in their inter-annual variation (Zou and Zhai 2004). Consequently, the NDVI data have been widely used for characterizing surface vegetation status (Kerr and Ostrovsky 2003; Thaim 2003; Weiss et al. 2004; Pettorelli et al. 2005; Telesca and Lasaponara 2006).

The purpose of this study is to re-delineate the dust source region in the extended model domain (Fig. 1) using the routinely (3 hourly) available World Meteorological Organization (WMO) surface reporting data, to determine the upper limit of the NDVI value for dust emission and to develop time-dependent dust emission

Fig. 1 The model domain and the distribution of WMO synoptic stations (filled triangle). The inner rectangle indicates the model domain of ADAM and ADAM1



reduction parameter with the use of spot/vegetation NDVI data for the period of 1998-2006. These results are used for the development of the ADAM2 model on the basis of the ADAM1 model. The potential of the ADAM2 model for the use of the Asian dust forecasting model is tested by simulating Asian dust events observed in Asia for the periods of 29 March to 2 April 2007 and of 29-31 December 2007.

2 Data

2.1 Normalized difference vegetation index

Spot/vegetation product of Maximum Value Composite Syntheses acquired in a 10-day period in a spatial resolution of $1 \times 1 \text{ km}^2$ in the Asian domain in Fig.1 is obtained from the site <http://free.vgt.vito.be/>.

The Spot 4 satellite has four vegetation spectral bands: the blue (BLU: $0.43\text{-}0.47 \mu\text{m}$), the red (RED: $0.61\text{-}0.68 \mu\text{m}$), the near infrared (NIR: $0.78\text{-}0.89 \mu\text{m}$), and MIR ($1.58\text{-}1.75 \mu\text{m}$).

The NDVI from Spot4/vegetation satellite datasets is defined as:

$$\text{NDVI} = \frac{\text{NIR} - \text{RED}}{\text{NIR} + \text{RED}}$$

with the pixel brightness count in the sea area being set to 0. The detailed NDVI datasets are given in Duchmin et al. (2000).

2.2 WMO synoptic data

Three-hourly reports of present weather, weather codes of 07 (blowing sand) and 08 (dust whirl) and wind speed at the WMO regular reporting stations in the domain of $70\text{-}150^\circ\text{E}$ and $5\text{-}60^\circ\text{N}$ (Fig. 1) for 9 years from 1998 to 2006 have been analyzed to identify occurrence locations and frequencies of Asian dust storms and dust rises. There are 821 regular reporting stations in the study domain (Fig. 1).

3 Model description

3.1 Meteorological model

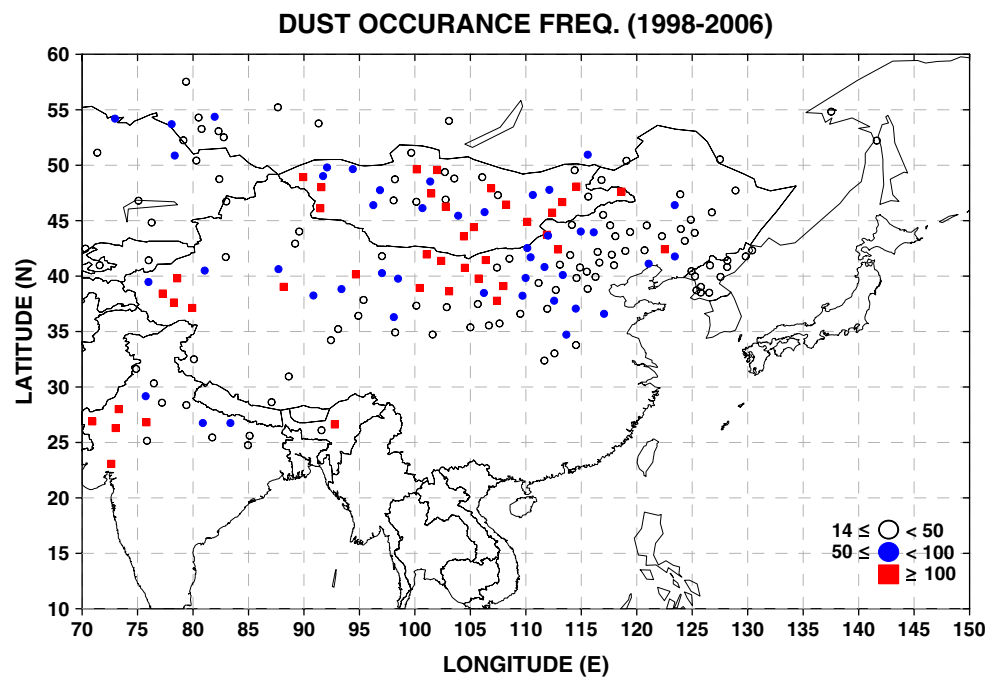
The meteorological model used in this study is the fifth generation mesoscale model of non-hydrostatic version (MM5, Pennsylvania State University/National Center for Atmospheric Research) defined in the x , y , and σ coordinate (Grell et al. 1994; Dudhia et al. 1998).

The model domain (Fig. 1) has a horizontal resolution of 30 km and 25 vertical layers including major Asian dust source regions (Fig. 2).

3.2 ADAM model

The ADAM model is an Eulerian dust transport model that includes the specifications of the dust source regions, delineated by the statistical analysis of the WMO dust

Fig. 2 The spatial distribution of the total number of dust rise reporting days for 9 years (1998–2006)



reporting data and the statistically derived dust emission conditions in sand, Gobi, loess, and mixed soil surface in the domain indicated by the inner rectangle in Fig. 1. The dust emission flux in the ADAM model is assumed to be proportional to the fourth power of the friction velocity and modified by the land use types in each source grid region. The ADAM model uses the suspended particle-size distribution parameterized by the several log-normal distributions of the soil particle-size distribution in the source regions, based on the concept of the minimally and fully dispersed particle-size distribution. It has 11 sizes of bins with near the same logarithm interval for particles of 0.15–37 μm in radius. The detailed description on the ADAM model is given in Park and In (2003) and Park and Lee (2004).

This ADAM model was modified to the ADAM1 model with the use of the observed meteorological parameters in the dust source regions and then to the ADAM2 model with the parameterized emission reduction factor using the NDVI data in the extended domain in Fig. 1.

4 The use of NDVI data for the modification of ADAM

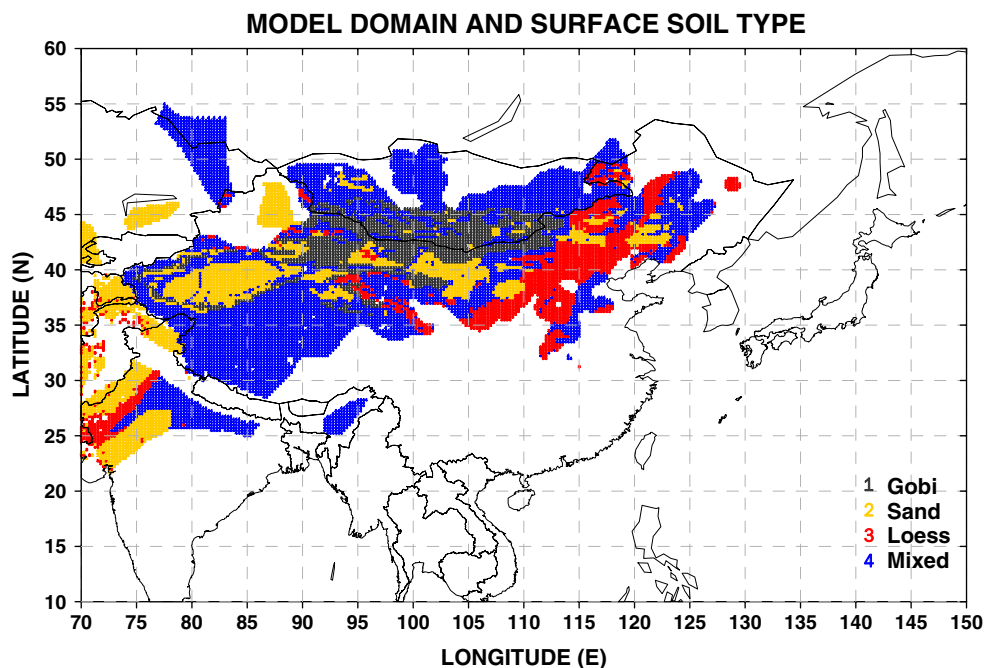
4.1 Re-delineation of Asian dust source regions

The method to delineate the Asian dust source regions is the same as in Park and In (2003) except for the extended region. Figure 2 shows the spatial distribution of the total

number of dust rise reporting days for 9 years from 1998 to 2006. The horizontal distribution pattern of the dust occurrence frequency shows maxima at the Tengger Desert (103.0–106.0°E, 38.5–39.6°N), Badain Jaran Desert (100.0–104.0°E, 39.5–41.3°N), and Mu Us Desert (108.0–110.0°E, 38.0–39.0°N), the Taklamakan Desert (76–88°E, 36.5–41.0°N), the northwestern part of India and the most parts of Mongolia. However, there is an increasing trend toward northeastward over the northeastern part of Inner Mongolia, Liaoning, and Jilin Province in China (not shown). This might be due to the desertification in the northeastern part of China. The horizontal distribution of the total number of dust rise occurrence days at a site, more than 14 days during last 9 years (Fig. 2) is used as the dust source regions. The choice of the dust rise occurrence frequency of 14 days per site for 9 years (1.6 days per year), which is equivalent to about 9% of the mean dust rise occurrence frequency (about 149 days per site for 9 years) at a site in the source region, is to reduce the dust rise reporting errors near the dust source regions.

However, the dust storms include not only the dust rise but also the blowing dust, so that Fig. 2 may not represent dust emission source regions. To delineate the emission source region of Asian dust, the soil-type map in the analysis domain has been introduced as in Park and In (2003). Figure 2 shows the spatial distribution of four different types of surface soils (Gobi, sand, loess, and mixed soil) in the dust emission regions that are identified with the soil-type map (Yi and Yaokun 1986) of each country.

Fig. 3 The spatial distribution of surface soil types (1 Gobi, 2 sand, 3 loess, 4 mixed) in the Asian dust source region



There are 167 regular reporting stations in the Asian dust source region of which 24, 29, 35, and 79 stations are located in the Gobi, sand, loess, and mixed soil regions, respectively (Figs. 2 and 3).

The 3-hourly reporting data at these stations are used to determine the dust emission conditions. Table 1 shows the total number of dust occurrence frequency in each month

and each surface soil type of the dust source region for 9 years (1998-2006).

Table 1 clearly indicates that the monthly variation of the dust occurrence frequency in the source region varies with the surface soil type. In the Gobi region, the monthly maximum dust occurrence frequency of 5.5/month/site occurs in April and then it decreases with time to a

Table 1 Total number of dust occurrence frequency in the source region for 9 years (1998-2006)

Month	Soil Site	Gobi 24	Sand 29	Loess 35	Mixed 79
1		121 (5.0)	92 (3.2)	69 (2.0)	145 (1.8)
2		324 (13.5)	305 (10.5)	81 (2.3)	268 (3.4)
3		533 (22.2)	760 (26.2)	525 (15.0)	759 (9.6)
4		1,193 (49.7)	1,442 (49.7)	706 (20.2)	1,367 (17.3)
5		612 (25.5)	1,846 (63.6)	420 (12.0)	822 (10.4)
6		354 (14.7)	1,601 (55.2)	227 (6.5)	300 (3.8)
7		253 (10.6)	1,177 (40.6)	54 (1.5)	76 (1.0)
8		168 (7.0)	607 (20.9)	10 (0.3)	124 (1.6)
9		195 (8.1)	191 (6.6)	12 (0.3)	236 (3.0)
10		211 (8.8)	74 (2.6)	20 (0.6)	186 (2.4)
11		171 (7.1)	85 (2.9)	50 (1.4)	168 (2.1)
12		141 (5.9)	90 (3.1)	37 (1.1)	131 (1.7)
Mean occurrence/year/site		19.8	31.7	7.0	6.5
Total area (km ²)		8.316×10 ⁵	1.482×10 ⁶	1.044×10 ⁶	3.62×10 ⁶

The number in the parenthesis indicates the average occurrence frequency per site for nine years. The area covering for each soil type is also indicated

minimum value of 0.6/month/site in next January. A relatively high dust occurrence frequency is seen in summer and autumn in the Gobi region. The annual mean dust occurrence frequency in the Gobi region is 19.8 per site.

In the sand region, the monthly mean maximum dust occurrence frequency of 7.1/year/site occurs in May and then it decreases rather quickly to reach minimum frequency of 0.3/year/site in October. The annual mean dust occurrence frequency (31.7/year/site) is the largest in the sand region compared with those in all other soil-type regions eventhough the dust occurrence frequency from October to next January is rather small.

In the loess and the mixed soil regions, the dust occurrence is mainly confined in the period of March through June with a maximum frequency in April in both regions. The annual mean dust occurrence frequencies are 7.0 and 6.5 per site in the loess and the mixed soil-type regions, respectively. These are rather smaller than those in the Gobi (19.8 per site) and sand (31.7 per site)

regions. This may be attributed to the crop land and the desertified grass/crop land in the loess and the mixed soil regions. During the winter, the frozen soil in the loess and mixed soil regions prevents the dust from rising while the growth of crops and/or grass after June makes it difficult to raise dust, resulting in a low dust occurrence frequency.

4.2 The threshold wind speed for the dust rise at each different surface soil type

The occurrence frequencies of wind speed, dust rise with respect to the wind speed, the ratio of the occurrence frequency of dust rise to that of the wind speed, and the normalized cumulative ratio of the occurrence frequency of the dust rise to that of the wind speed with respect to the wind speed in various soil-type regions are examined for each month for the period of 9 years (1998-2006). The threshold wind speed is defined as the wind speed at the normalized cumulative ratio of the dust occurrence fre-

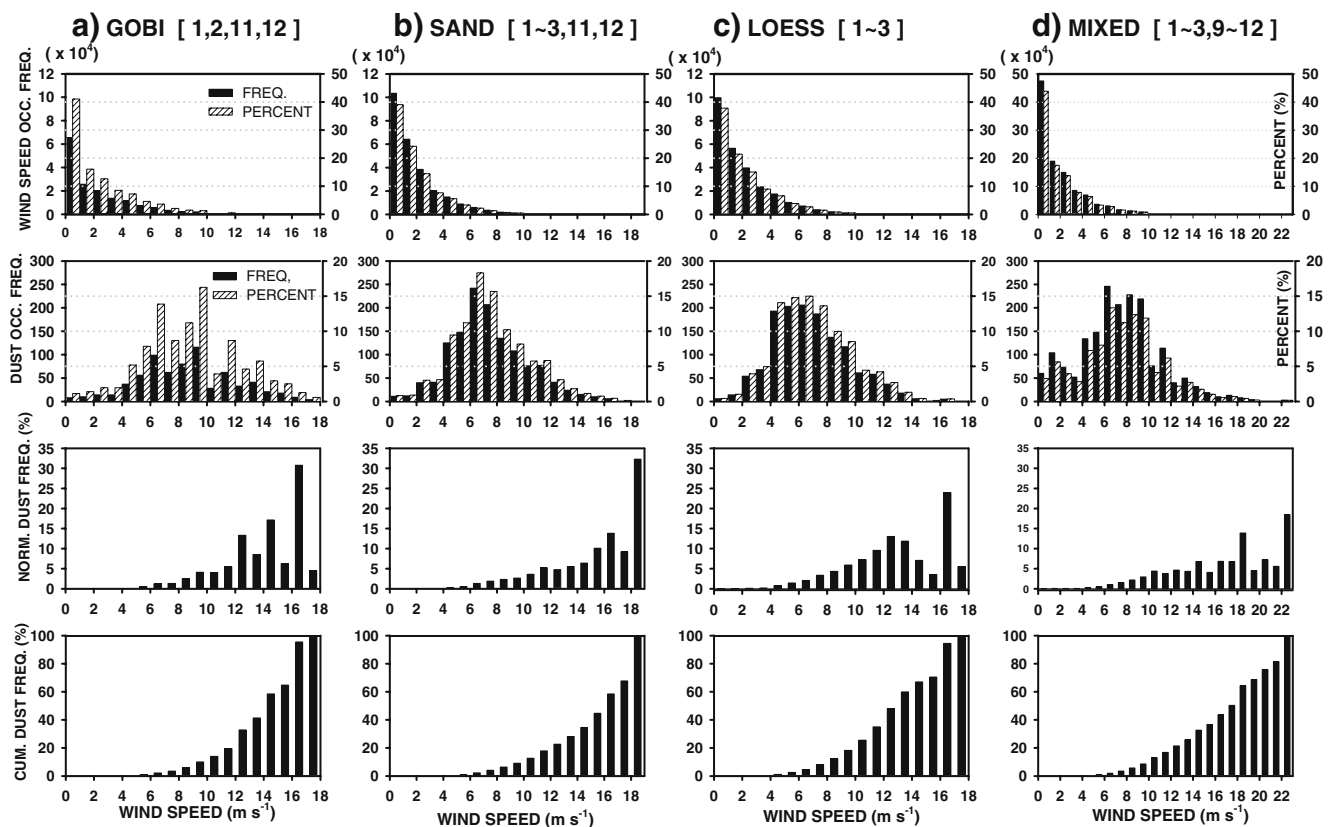


Fig. 4 Occurrence (*shaded bar*) and percent frequencies (*hatched bar*) of the wind speed, dust rise, percent ratio of the occurrence frequency of dust rise to that of wind speed and the normalized cumulative dust occurrence percentage with respect to the wind speed in the interval of 1 m s^{-1} for the period of **a** January, February,

November, and December in the Gobi; **b** January to March and November and December in sand; **c** January through March in the loess; and **d** January to March and September through December in the mixed-soil regions

Table 2 Monthly variations of the threshold wind speed (m s^{-1}) in each soil-type region

Month	Soil	Gobi	Sand	Loess	Mixed
1		8.0	7.5	6.0	7.5
2		8.0	7.5	6.0	7.5
3		7.0	7.5	6.0	7.5
4		7.0	6.0	5.5	6.0
5		7.0	6.0	5.0	6.0
6		7.0	6.0	5.0	6.0
7		7.0	6.0	–	6.0
8		7.0	6.0	–	6.0
9		7.0	6.0	–	7.5
10		7.0	6.0	–	7.5
11		8.0	7.5	7.5	7.5
12		8.0	7.5	7.5	7.5
ADAM		9.5	7.5	6.0	9.2

The value used in the ADAM model is also listed

quency being 3.5% (Park and In 2003). This means that the threshold wind speed for the dust rise larger than 1.95 standard deviation of the dust rise probability function is considered to be erroneous data.

The estimated monthly threshold wind speed shows a nearly the same value for a certain time period of the

Table 3 The free NDVI value (FNV) in each soil-type region

Soil Type	Gobi	Sand	Loess	Mixed
FNV	0.09	0.21	0.19	0.17

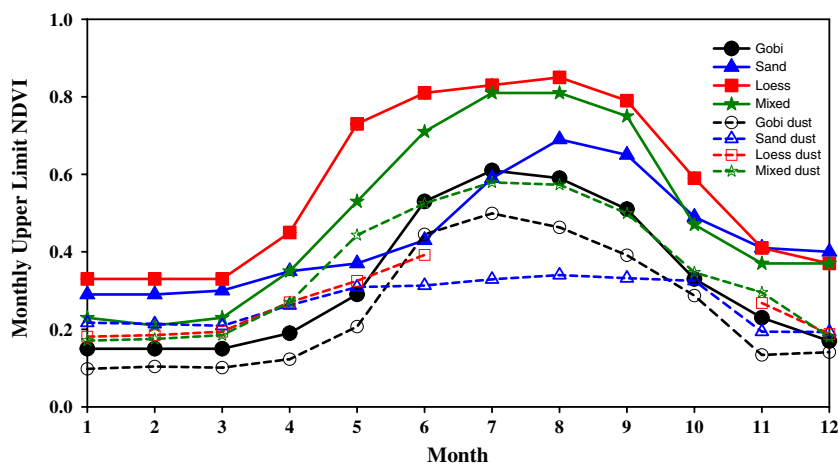
year. Therefore, the threshold wind speed is estimated with occurrence frequencies of the wind speed and the dust rise for several months rather than for each month in each soil-type region.

Figure 4 shows occurrence and percent frequencies of wind speed, dust rise, the percent ratio of the occurrence frequency of dust rise to that of the wind speed, and the normalized cumulative dust occurrence percentage with respect to the wind speed in an interval of 1 ms^{-1} in the months of January, February, November, and December in the Gobi region (Fig. 4a), January to March, November and December in the sand region (Fig. 4b), January to March in the loess region (Fig. 4c), and January to March, September to December in the mixed soil-type region (Fig. 4d). The threshold wind speeds estimated by using the above mentioned criteria yield 8.0, 7.5, 6.0, and 7.5 ms^{-1} in the Gobi, sand, loess, and mixed soil region, respectively.

The same method is applied to the other months for the different soil types. The results are given in Table 2.

The threshold wind speed in the loess region for the period of July to October cannot be resolved due to very few dust rise occurrence frequencies (Table 1). The presently estimated threshold wind speeds in the Gobi and the mixed soil-type region are 1.5-3 ms^{-1} lower than those values used in ADAM (Park and In 2003; Park and Lee 2005) that is used as an operational model in KMA.

Fig. 5 Monthly variations of the upper limit value of NDVI determined by the threshold wind speed (solid lines) and by the dust occurrence frequency (dashed lines) in the Gobi (filled circle, empty circle), sand (filled triangle, empty triangle), loess (filled square, empty square), and mixed soil (filled square, empty square) regions



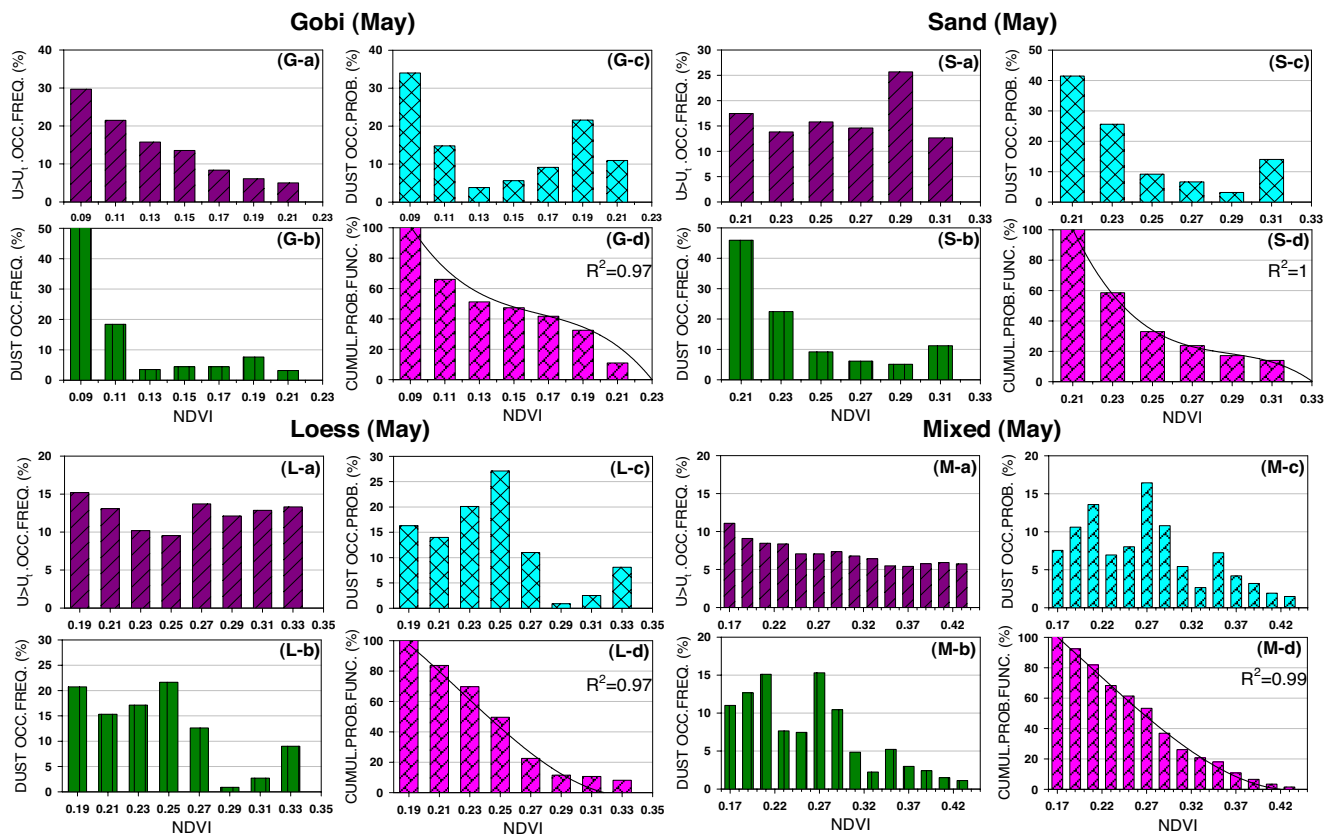
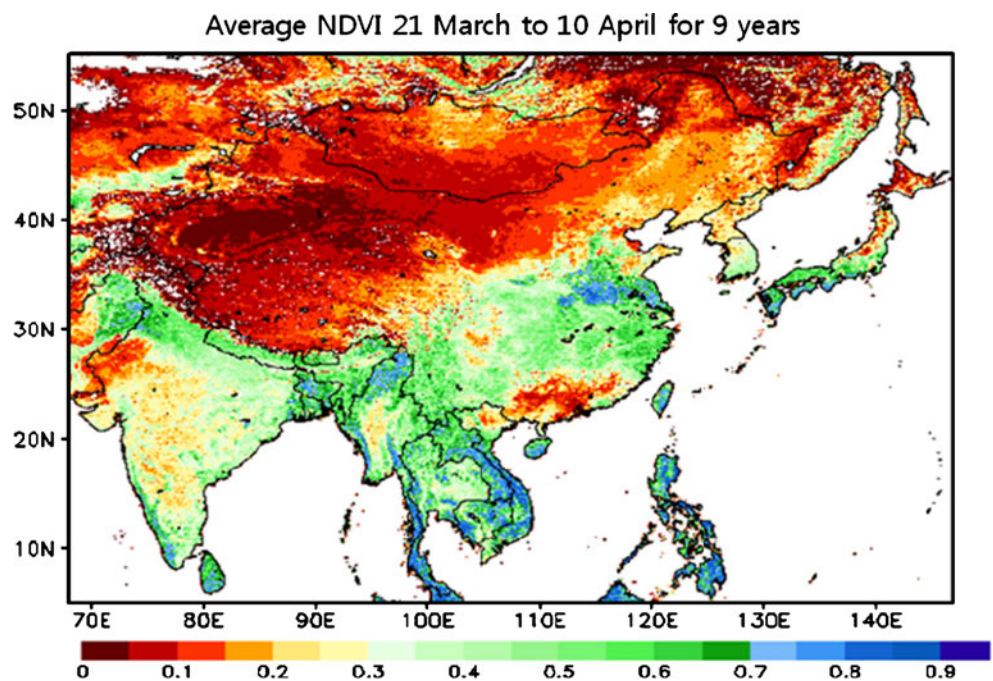


Fig. 6 Normalized percent occurrence frequencies of **a** the wind speed exceeding the threshold wind speed, **b** dust rises, **c** percent ratio of **b** to **a**, and **d** the cumulative dust occurrence probability function in

the Gobi (G), sand (S), loess(L), and mixed (M) soil-type region. The cubic spline fitted cumulative dust occurrence probability functions with R^2 values are indicated in **d**

Fig. 7 The spatial distribution of NDVI averaged for the period from 21 March to 10 April for 9 years (1998-2006)



4.3 Monthly variation of the upper limit value of NDVI in the Asian dust source region

The NDVI values obtained from spot/vegetation product in the Asian dust source region (Fig. 3) are used for the analysis. From these data, nine NDVI values of data centered at each WMO surface-reporting station are retrieved for 9 years from 1998 to 2006 to find occurrence frequency of the NDVI value with respect to the NDVI value in an interval of 0.01 in each surface soil-type region (Fig. 3). Among these data, the NDVI data are chosen when the wind speed reported at that station exceeds the threshold wind speed in Table 2, and then the distribution

of the occurrence frequency of the NDVI value with respect to the NDVI value in an interval of 0.01 is made for each month. The occurrence frequency of the NDVI value in each interval is normalized by dividing the total number of occurrence frequency in the whole range of the NDVI value. The upper limit value of NDVI is determined as the NDVI value at the normalized cumulative NDVI occurrence frequency being 99% for each month in each surface soil-type region.

Figure 5 shows the monthly variation of the mean upper limit value of NDVI in different soil-type regions. During the winter from November to March, the upper limit value of NDVI is almost constant in each soil-type

Fig. 8 The spatial distribution of the dust emission reduction factor for the period of 21 March to 10 April. The meteorological monitoring tower site (multiplication symbol), PM₁₀ monitoring site in China (filled diamond) and the enhanced South Korea map with PM₁₀ monitoring sites (filled circle) are indicated

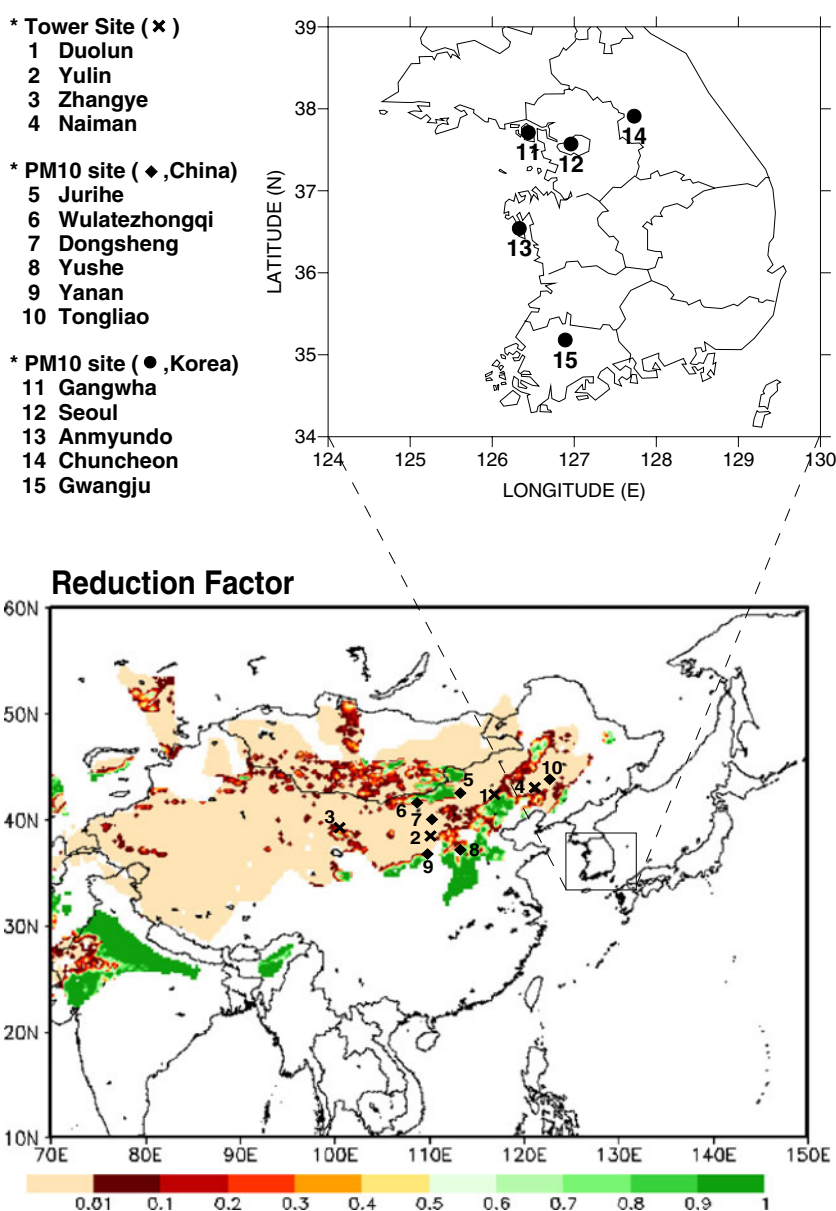
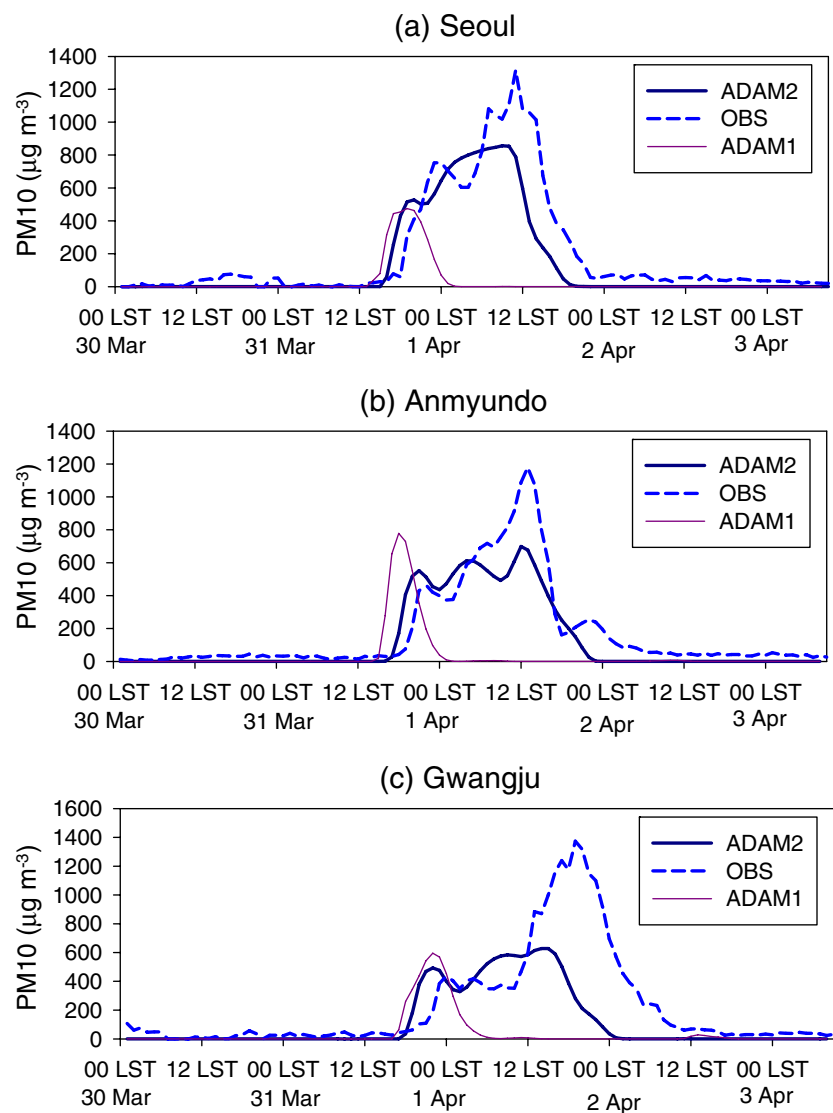


Fig. 9 Time series of the ADAM1 (*thin solid line*), ADAM2 (*thick solid line*), and observed (*broken line*) PM₁₀ concentration ($\mu\text{g m}^{-3}$) at **a** Seoul, **b** Anmyundo, and **c** Gwangju in Korea for the period 30 March–3 April 2007



region with the minimum of 0.15 in the Gobi region, whereas the maximum value of 0.32 in the loess region. As the season progresses, the upper limit value of NDVI becomes large to reach a maximum value of 0.61 in July and August in the Gobi region, 0.70 in August in the sand region, 0.83 in August in the loess region, and 0.81 in July in the mixed soil region. This might be associated with the growth of vegetation in these regions.

Similar analyses have been done for the dust occurrence with respect to the NDVI value in the interval of 0.01. The result is also shown in Fig. 5 as dashed lines. The upper limit value of NDVI for the dust occurrence varies quite similarly with that for the NDVI occurrence frequency (solid lines in Fig. 5) but much lower value of NDVI during the vegetation growing season in each

soil-type region. However, the upper limit value of NDVI for the dust occurrence in the loess region cannot be resolved during the summer season due to the lack of dust occurrence frequency data. This implies that the probability of dust occurrence in the loess region during the summer is very small.

It is worthwhile to note that during the winter time when the vegetation is rare (or bare soil) the upper limit value of NDVI for the dust occurrence is minimum. However, this minimum value varies with the surface soil type. This allows defining the “free NDVI value (FNV)” for each soil type. In other words, it means the upper limit value of NDVI for the dust occurrence without the impact of the vegetation. Table 3 shows the free NDVI value for the dust occurrence in each soil-type region.

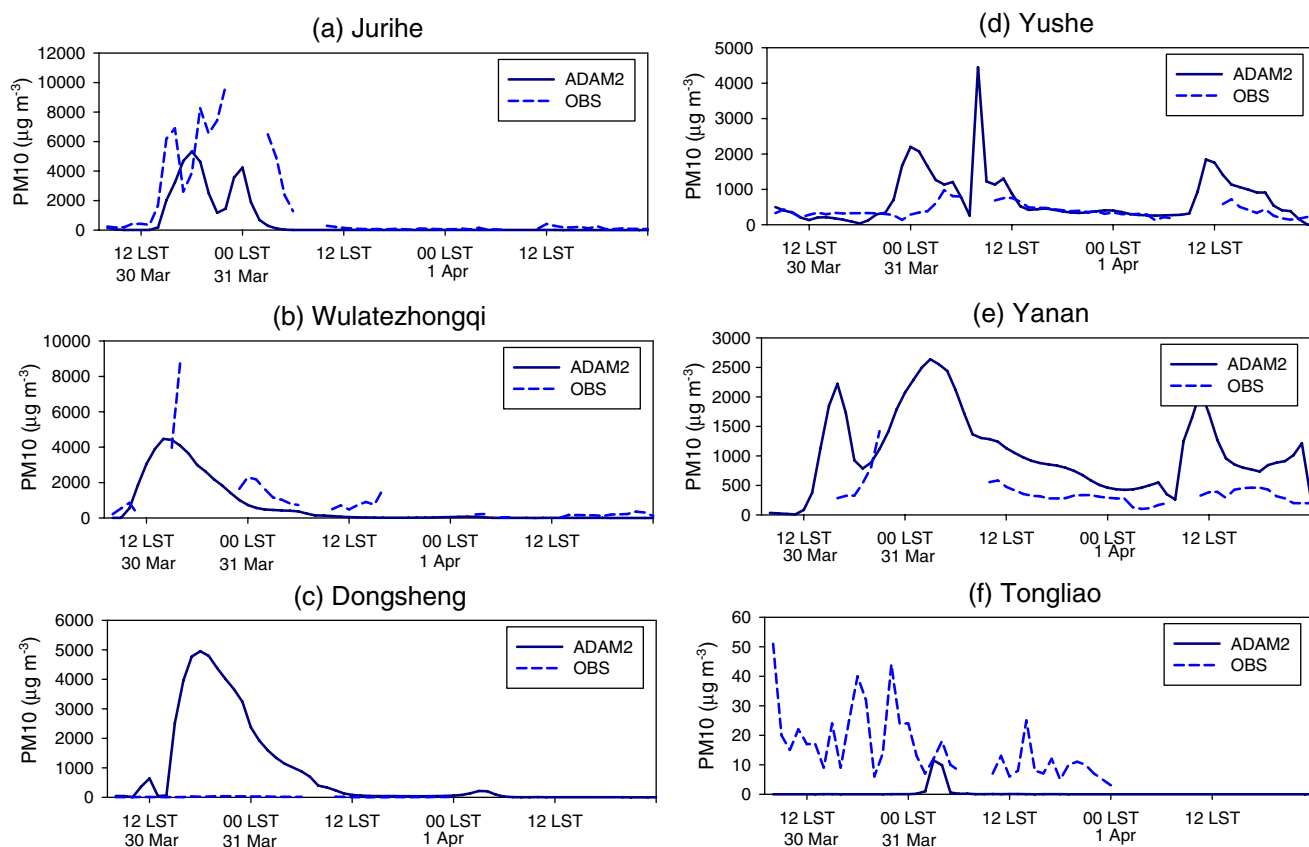


Fig. 10 Time series of the ADAM2(*thick solid line*) and observed (*broken line*) PM₁₀ concentration (µg m⁻³) at **a** Jurihe, **b** Wulatezhongqi, **c** Dongsheng, **d** Yushi, **e** Yanan, and **f** Tongliao in China for the period 30 March-1 April 2007

4.4 The parameterization of the dust emission reduction factor using the NDVI value

The vegetation in the dust source region reduces the occurrence of the dust events (Fig. 5). The impact of vegetation on the dust occurrence can be estimated by analyzing the occurrence frequencies of the NDVI value and the dust rise in the NDVI range from the FNV (Table 3) to the upper limit value of NDVI (UNV) for the dust occurrence (Fig. 5).

Figure 6 shows, for one example, the procedure to get the dust occurrence probability function (P_0) affected by the vegetation in each soil-type region in May. We construct the distributions of the normalized NDVI occurrence frequency that exceeds the threshold wind speed (Fig. 6 (G-a)) and the normalized the dust occurrence frequency (Fig. 6 (G-b)) in the range from FNV to the upper limit value of NDVI for the dust occurrence (UNV) in the interval of 0.01. And then the dust occurrence probability function (Fig. 6 (G-c)) is calculated by dividing the distribution function of the normalized dust occurrence frequency

(Fig. 6 (G-b)) by that of the normalized NDVI occurrence frequency (Fig. 6 (G-a)). And then the resulting distribution is normalized by dividing the total sum of the percentage distribution from FNV to UNV in Fig. 6 (G-c). The probability density function (Fig. 6 (G-d)) affected by vegetation is obtained from the cumulative probability function of the dust occurrence probability function in Fig. 6 (G-c). The analytical dust occurrence probability density function (P_0) is obtained by fitting a cubic spline function to the distribution of the cumulative probability density function to satisfy the conditions of $P_0=1$ at FNV and $P_0=0$ at UNV. This function is shown in Fig. 6 (G-d) in the Gobi region. The same method has been employed in other soil-type regions (Fig. 6 (S, L, and M)) to get the function P_0 .

Thus the dust emission reduction factor R is given by

$$R = \begin{cases} 0 & \text{for NDVI} \leq \text{FNV} \\ 1 - P_0 & \text{for FNV} < \text{NDVI} < \text{UNV} \\ 1 & \text{for NDVI} \geq \text{UNV} \end{cases} \quad (1)$$

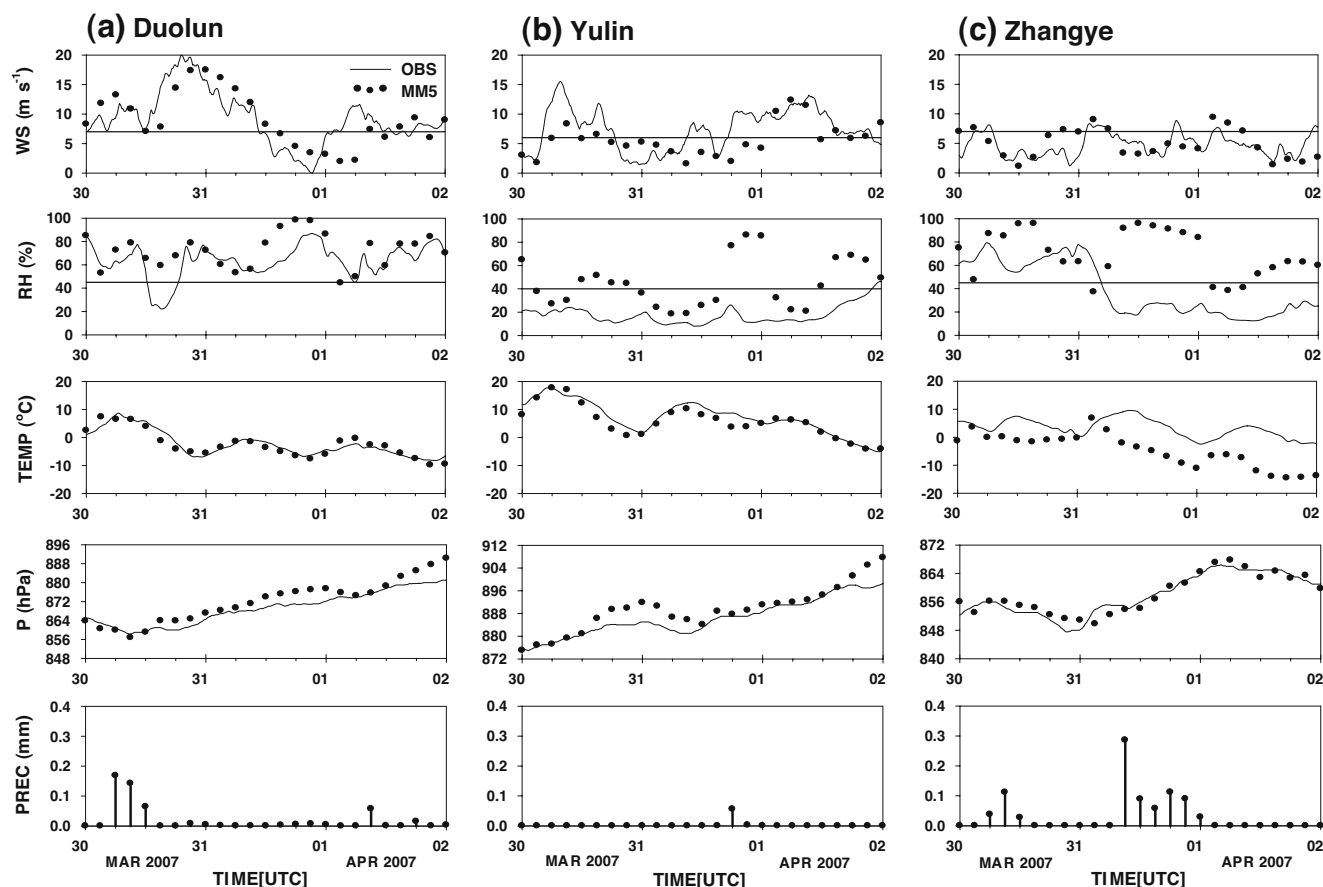


Fig. 11 Time series of observed (*thick solid line*) and modeled (*dotted line*) wind speed (m s^{-1}), relative humidity (%), temperature ($^{\circ}\text{C}$), surface pressure (hPa), and 3-h accumulated precipitation (mm) at **a** Duolun, **b** Yulin, and **c** Zhangye in the Asian dust source region for

the period 30 March to 2 April 2007. The *horizontal line* in the wind speed is the threshold wind speed and that in the relative humidity is the upper limit value of the dust rise

The statistically determined dust occurrence probability density function in the NDVI range from FNV to UNV with the R^2 value are given in the [Appendix](#). This allows us to run the model all year round using the different reduction factor in each month in each soil-type region that is not available in the ADAM model.

5 Simulations of Asian dust events observed on 31 March to 2 April and 29–31 December 2007 in Korea with the modified ADAM model (ADAM2)

The ADAM1 model (Park and Lee, 2005) has been modified to the “ADAM2 model” with presently developed emission reduction factors derived from NDVI value in [Appendix](#) and the renewed threshold wind speed (Table 2) in the extended model domain (Fig. 1).

5.1 The Asian dust event observed on 31 March to 2 April 2007 (a spring dust event)

The ADAM2 model has simulated an Asian dust event observed in Korea on 31 March to 2 April 2007 with the use of the NDVI distribution averaged for the period of 20 March to 10 April for 9 years (1998–2006) in the Asian dust source region. The spatial distribution of averaged NDVI for this period is given in Fig. 7 and that of the emission reduction factor due to vegetation estimated by Eq. 1 with the use of the empirical equation in the [Appendix](#) in the Asian dust source region is given in Fig. 8.

Much of the Asian dust source regions during this time period show the NDVI value less than 0.2 except in Northern India where the NDVI value is larger than 0.6 (Fig. 7). Consequently, the emission reduction factor due to vegetation is almost negligible in most parts of the

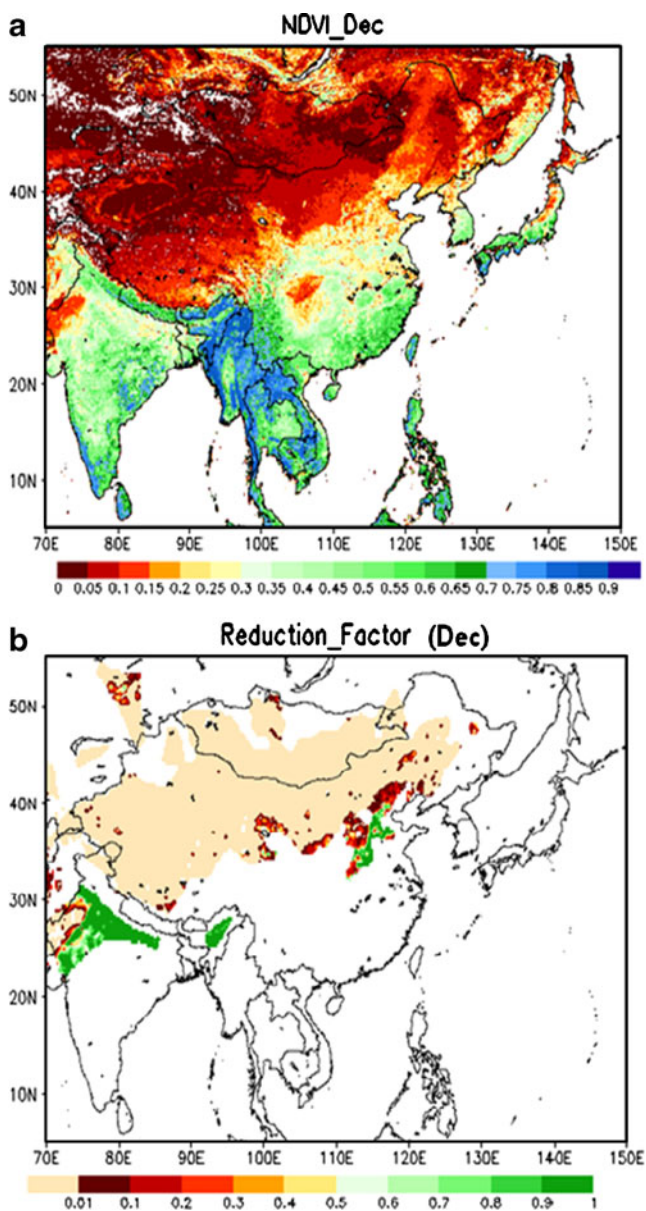


Fig. 12 The spatial distributions of **a** NDVI and **b** reduction factor averaged for the month of December for 9 years (1998-2006)

source region in Northern China while most of dust emission regions in Northern India and small fractions of the southeastern part of Mongolia over the sand desert area and the central eastern part of China over the loess and mixed soil region can be suppressed by vegetation (Fig. 8).

Figure 9 shows time series of observed and simulated PM₁₀ concentrations for this dust event at several sites in Korea (Fig. 8). The simulation has been done with the ADAM1 model (thin solid line in Fig. 9) and the ADAM2 model (thick solid line in Fig. 9). Both models success-

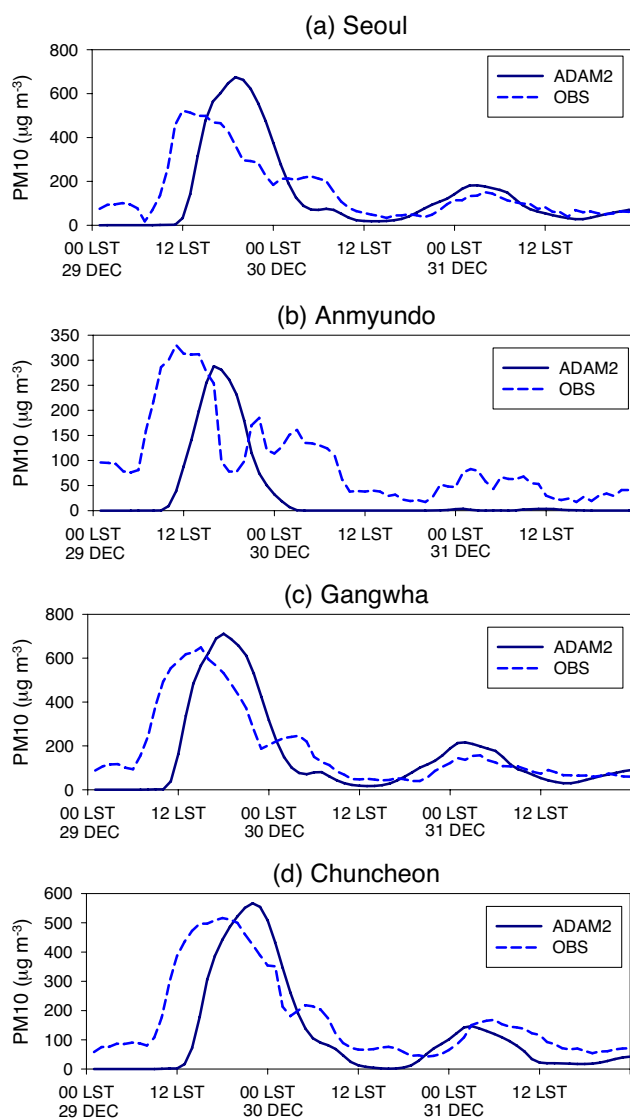


Fig. 13 Time series of observed (*thick solid line*) and modeled (*broken line*) PM₁₀ concentration ($\mu\text{g m}^{-3}$) at **a** Seoul, **b** Anmyundo, **c** Ganghwa, and **d** Chuncheon in Korea for the period 29–31 December 2007

fully simulate the starting time of the Asian dust event observed in Korea. However, the ADAM1 model cannot simulate the duration period of the Asian dust event observed in Korea, whereas the presently modified ADAM2 model simulates quite well the first peak concentration but the second maximum peak concentration is much underestimated at all sites with a little short time duration period of the dust event (Fig. 9).

Figure 10 shows time series of observed and simulated PM₁₀ concentration at several sites in the dust source region of China (Fig. 8). There are so many missing and/or incorrect data in the observed PM₁₀ concentrations in the

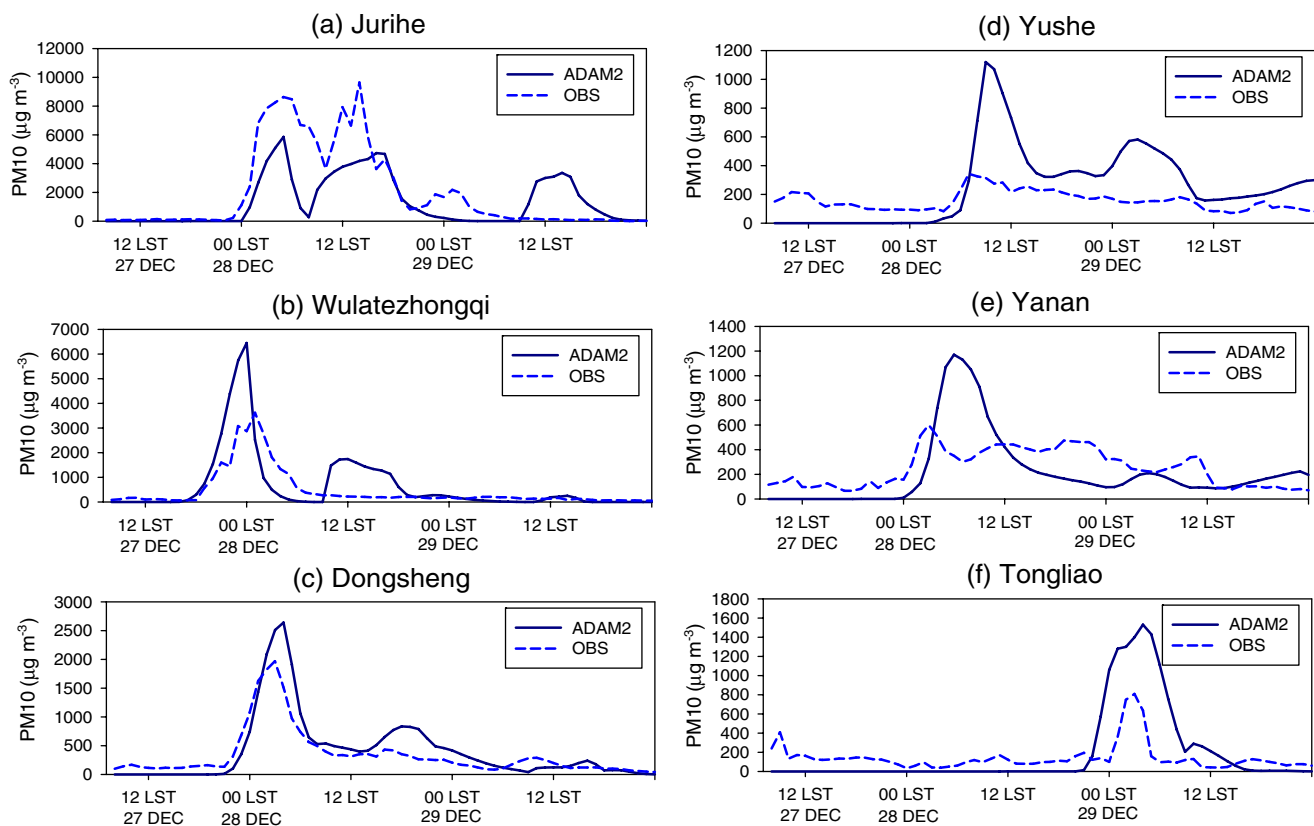


Fig. 14 The same as in Fig. 10 except for the period 27–30 December 2007

source region that it is difficult for the model result to be compared with observations. However, there are similar time variations between the modeled and observed PM_{10} concentration in the source regions.

Meteorological variables obtained from the monitoring towers in the dust source regions (Fig. 8) are compared with the model results and given in Fig. 11. The 10-min averaged wind speed, relative humidity, and temperature (Figs. 11a–c) are obtained at the height of 16 m from the 20-m monitoring tower. These data are averaged by taking a 1 h running mean. The results are compared with the results of the lowest level of the model (about 15 m above the ground). Both the modeled and the observed surface pressure (Fig. 11d) are taken at the surface and the precipitation (Fig. 11e) is the 3-h accumulated amount.

The MM5 simulated wind speed, temperature, and pressure are quite similar to those observations at Duolun (Fig. 11a) but the model overestimates the relative humidity and the occurrence frequency of precipitation. The tower observed meteorological data satisfy the dust emission conditions for the time period of 08:00–12:00 Coordinated Universal Time (UTC) on 30 March but the model fails to

dust emission for this time period due to overestimation of relative humidity.

At Yulin (Fig. 11b), the model simulates quite well the temperature and surface pressure but overestimates the relative humidity and the occurrence frequency of precipitation, whereas the wind speed is slightly underestimated. The dust emission conditions are satisfied by the observed meteorological fields for the periods of 08:00–18:00 UTC on 30 March and 18:00 UTC on 31 March to 12:00 UTC on 1 April. However, the model satisfies the dust emission conditions for the periods of 08:00–12:00 UTC on 30 March and 00:00–12:00 UTC on 1 April. Due to the overestimated relative humidity by the model, the dust emission period simulated by the model is shorter than that of the observation (Fig. 11b).

At Zhangye (Fig. 11c), the model simulates quite well the surface pressure and wind speed. However, the relative humidity and precipitation frequency are highly overestimated. On the other hand, the simulated temperature is underestimated. However, both the model and observation satisfy the dust emission conditions for the periods of 01:00–03:00 UTC on 31 March and 01:00–04:00 UTC on 1 April.

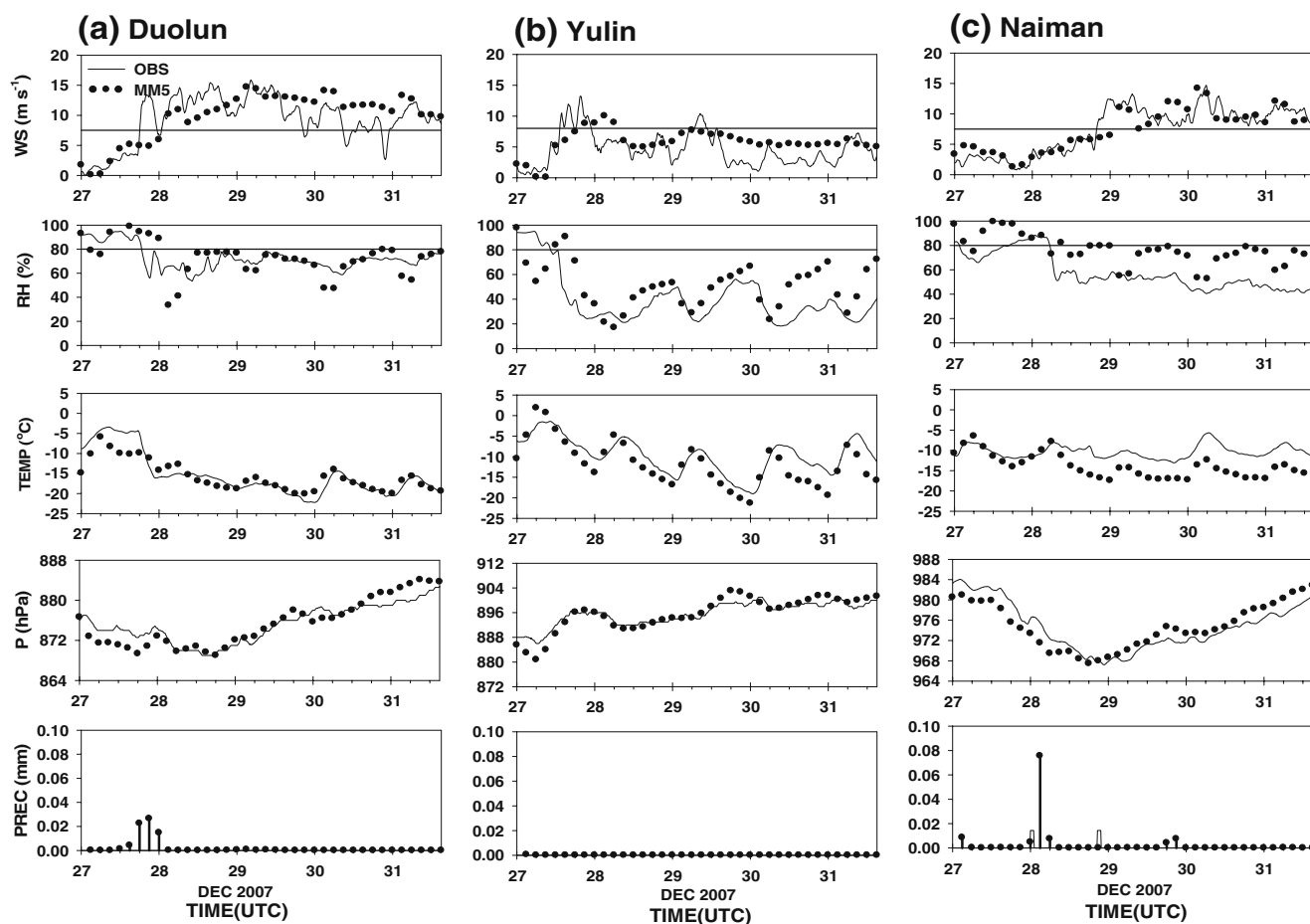


Fig. 15 The same as in Fig. 11 except for **a** Duolun, **b** Yulin, and **c** Naiman for the period 27–31 December 2007

5.2 The Asian dust event observed on 29–31 December 2007 (a winter dust event)

The performance test of the ADAM2 has been conducted for an Asian dust event occurred during the winter (29–31 December 2007).

The spatial distributions of averaged NDVI for the month of December for 9 years (1998–2006) and the corresponding emission reduction factor due to vegetation in the source region are given in Fig. 12.

The most of Asian dust source regions in December (Fig. 12a) shows the NDVI value <0.15 which is slightly lower than that in spring (Fig. 7). Consequently, the dust emission reduction due to vegetation is almost negligible in most parts of the source region (Fig. 12b) except in the subtropical region of Northern India where the dust emission is largely suppressed by vegetation.

Figure 13 compares the observed surface PM_{10} concentration at several monitoring sites in Korea (Fig. 8) with the simulated one by the ADAM2 model simulated

PM_{10} concentration. The model simulates almost the same magnitude of the observed PM_{10} concentration at all monitoring sites in Korea. However, the starting time of the Asian dust event in Korea is lagged about 3–4 h (likewise the peak concentration occurring time). This is attributed to the rather slow movement of a dust-loaded synoptic system in the dust-source region toward the Korean peninsula (not shown here), suggesting the importance of accurate simulation of meteorological fields.

Figure 14 shows the simulated and observed surface PM_{10} concentration at several sites in the dust source region of China (Fig. 8). The model simulates quite well the time variation of the observed PM_{10} concentration at all sites in China. However, the model slightly overestimates the first PM_{10} concentration peak at all monitoring sites except at Jurihe (Fig. 14a) where the PM_{10} concentration is slightly underestimated.

Figure 15 shows tower measurements of meteorological fields with the model results in the dust source region for the period of 27–31 December 2007.

At Duolun (Fig. 15a), the model simulates quite well the relative humidity, temperature, and surface pressure with slightly overestimated wind speed. The model produces falsely precipitation for the period of 15:00–24:00 UTC on 27 December. The model satisfies the dust emission conditions for a short time period from 01:00–04:00 UTC on 28 December but there is no time period to satisfy the dust emission conditions in the observed data.

At Yulin (Fig. 15b), the model simulates quite well the surface pressure and precipitation but slightly underestimates the temperature. The wind speed and the relative humidity are slightly overestimated. There are two periods to satisfy the dust emission conditions. One is from 10:00 UTC to 14:00 UTC on 27 December and the other from 01:00–06:00 UTC on 29 December in the observed data whereas the modeled data shows that the first one is lagged by 3 h and the second one occurs almost the same time period.

At Naiman (Fig. 15c), the model successfully simulates the surface pressure but slightly overestimates the wind speed, relative humidity, and the precipitation occurrence frequency. The temperature is slightly underestimated. Both the observed and modeled data satisfy the dust emission condition for the period of 01:00–04:00 UTC on 30 December.

6 Summary and conclusions

The operational ADAM1 in KMA has been modified to the ADAM2 model. The modification has been done by re-delineating the Asian dust source region in the extended model domain (70–160°E and 5–60°N), with the temporal variations of the threshold wind speed for the dust rise in each soil-type region using the routinely available WMO surface reporting data and the parameterized time-dependent dust emission reduction factor due to the vegetation with the use of spot/vegetation NDVI data for the period of 1998–2006. The modified-ADAM2 model has been implemented to simulate Asian dust events observed in Korea for the periods of 31 March to 2 April 2007 (a spring dust event) and 27–31 December 2007 (a winter dust event) when the observed PM₁₀ concentration at some monitoring sites in the source region exceeded 9,000 µg m⁻³.

It is found that the threshold wind speed for the dust rise varies significantly with time and surface soil types with the highest threshold wind speed (8.0 ms⁻¹) in the Gobi region and the lowest (6.0 ms⁻¹) in the Loess region. In all different soil-type regions, the threshold wind speed during the winter time is found to be stronger than that during the

summer time, suggesting the importance of the convective velocity for the dust rise in summer.

The statistical analysis of the spot/vegetation NDVI data is able to determine the FNV which is defined as the NDVI value without the effect of vegetation in different soil-type regions and the UNV for the dust rise. The statistically obtained FNVs are found to be 0.09, 0.21, 0.19, and 0.17 in Gobi, sand, loess, and mixed soil regions, respectively. However, UNVs vary according to the growth of vegetation in each soil-type region. The dust emission reduction factor due to vegetation that is derived from the 24 categories of the USGS land-use types and used as a fixed value in time in the ADAM1 model (Park and In, 2003; Park and Lee, 2004), is parameterized with the use of the dust occurrence probability function derived from the values of FNV and UNV for the dust rise in each soil-type region. This enables to run the model all year round with time-dependent different emission reduction factor in each soil-type region.

The presently modified ADAM2 model is found to simulate quite well the starting time and the first peak PM₁₀ concentration of the Asian dust event in spring observed in Korea. However, the second maximum PM₁₀ concentration observed in Korea is underestimated due to the failure of the correct simulation of the meteorological fields. However, the dust concentration in the dust source region is found to be simulated quite well. The dust event in winter (27–31 December 2007) is found to be well simulated by the ADAM2 model in terms of dust concentrations in the dust source region of China and the downstream region of Korea. However, the starting time of the dust event in the downstream region of Korea is lagged by 3–4 h due to the slow movement of a dust loaded synoptic system. This suggests that the ADAM2 model has a great potential to be used as an operational forecasting model in Asia provided more accurate meteorological fields.

The present study mainly pertains to the modification of the ADAM1 model to the ADAM2 model by renewing the time-dependent threshold wind speed and the dust emission reduction factor due to vegetation so as to be able to run the model all year round in the Asian domain. More accurate prediction of the dust concentration requires a proper parameterization of dust emission processes. This is now on hand.

Acknowledgments This work was funded by the Korea Meteorological Administration Research and Development Program under Grant CATER 2008-3208. Thanks are given to four anonymous reviewers for their helpful comments.

Appendix The dust occurrence probability density function ($P_0 = a_0 + a_1x + a_2x^2 + a_3x^3$) with the R^2 value, free NDVI value (FNV) and upper limit value of NDVI for dust occurrence (UNV) in the Gobi, Sand, Loess, and mixed-soil region

Soil type Month		Gobi				Sand			
		P_0	R^2	FNV	UNV	P_0	R^2	FNV	UNV
1	—	—	0.09	0.09	—	—	0.21	0.21	
2	—	—	0.09	0.09	—	—	0.21	0.21	
3	—	—	0.09	0.09	—	—	0.21	0.21	
4	$a_0=-38.55, a_1=1162.90$ $a_2=-11130.01, a_3=34351.49$	1	0.09	0.13	$a_0=211.71, a_1=-2533.77$ $a_2=10113.24, a_3=-13455.69$	1	0.21	0.27	
5	$a_0=4.81, a_1=-73.96$ $a_2=431.95, a_3=-874.98$	0.97	0.09	0.23	$a_0=33.79, a_1=-345.72$ $a_2=1192.16, a_3=-1378.20$	1	0.21	0.33	
6	$a_0=1.63, a_1=-9.87$ $a_2=31.59, a_3=-38.20$	0.99	0.09	0.47	$a_0=39.55, a_1=-428.18$ $a_2=1567.02, a_3=-1917.57$	0.99	0.21	0.33	
7	$a_0=1.22, a_1=-4.14$ $a_2=14.54, a_3=-21.75$	0.98	0.09	0.51	$a_0=31.91, a_1=-327.05$ $a_2=1128.93, a_3=-1299.79$	0.98	0.21	0.35	
8	$a_0=1.43, a_1=-7.56$ $a_2=32.40, a_3=-48.54$	0.99	0.09	0.47	$a_0=-7.41, a_1=116.19$ $a_2=-498.96, a_3=650.03$	0.97	0.21	0.35	
9	$a_0=1.11, a_1=-1.51$ $a_2=-0.26, a_3=-6.54$	0.97	0.09	0.41	$a_0=11.38, a_1=-92.24$ $a_2=252.60, a_3=-233.99$	0.98	0.21	0.35	
10	$a_0=1.76, a_1=-14.62$ $a_2=80.77, a_3=-168.29$	0.99	0.09	0.31	$a_0=22.89, a_1=-236.80$ $a_2=841.80, a_3=-1006.10$	0.96	0.21	0.35	
11	$a_0=-17.38, a_1=508.92$ $a_2=-4532.62, a_3=12749.25$	1	0.09	0.15	—	—	0.21	0.21	
12	—	—	0.09	0.09	—	—	0.21	0.21	
Soil type Month		Loess				Mixed			
		P_0	R^2	FNV	UNV	P_0	R^2	FNV	UNV
1	—	—	0.19	0.19	—	—	0.17	0.17	
2	—	—	0.19	0.19	—	—	0.17	0.17	
3	—	—	0.19	0.19	—	—	0.17	0.17	
4	$a_0=-12.61, a_1=196.99$ $a_2=-907.35, a_3=1303.86$	1	0.19	0.29	$a_0=467.35, a_1=-3984.56$ $a_2=14286.50, a_3=-21047.23$	0.97	0.17	0.29	
5	$a_0=-0.05, a_1=28.43$ $a_2=-169.37, a_3=252.90$	0.97	0.19	0.35	$a_0=1.62, a_1=-1.08$ $a_2=-20.85, a_3=33.86$	0.99	0.17	0.45	
6	$a_0=6.66, a_1=-51.04$ $a_2=134.24, a_3=-120.59$	1	0.19	0.41	$a_0=2.31, a_1=-9.80$ $a_2=14.62, a_3=-8.14$	0.99	0.17	0.55	
7	—	—	0.19	—	$a_0=2.13, a_1=-10.07$ $a_2=26.68, a_3=-28.03$	0.98	0.17	0.55	
8	—	—	0.19	—	$a_0=0.45, a_1=6.70$ $a_2=-23.18, a_3=17.88$	0.98	0.17	0.59	
9	—	—	0.19	—	$a_0=0.68, a_1=4.96$ $a_2=-21.31, a_3=17.56$	0.99	0.17	0.51	
10	—	—	0.19	—	$a_0=3.87, a_1=-28.96$ $a_2=88.75, a_3=-104.72$	0.99	0.17	0.37	
11	$a_0=7.68, a_1=-82.42$ $a_2=344.00, a_3=-528.60$	0.93	0.19	0.29	$a_0=9.81, a_1=-116.90$ $a_2=510.68, a_3=-747.30$	0.98	0.17	0.33	
12	—	—	0.19	0.19	—	—	0.17	0.17	

References

- Duchmin B, Maisongrande P, Dedieu G, Leroy M, Roujean JL, Bicheron P, Hauteceur O, Lacaze R (2000) A 10-day compositing method accounting for bidirectional effects. *Proceedings of the VEGETATION 2000*: 313–318, Belgirate, Italy
- Dudhia J, Grill D, Guo Y-R, Hausen D, Manning K, Wang W (1998) PSU/NCAR mesoscale modeling system tutorial class notes (MM5 modeling system version 2)
- Gillette DA (1981) Production of dust that maybe carried great distances. *Spec Pap Geol Soc Am* 186:11–26
- Grell GA, Dudhia J, Stauffer DR (1994) A description of the 5th generation Penn State/NCAR mesoscale model (MM5). NCAR TECH. Note NCAR/TN-398, 117 pp
- Huang S, Siegert F (2006) Land cover classification optimized to detect areas at risk of desertification in North China based on SPOT VEGETATION imagery. *J Arid Environ* 67:308–327
- Husar RB, Tratt DM, Schichtel BA, Falke SR, Li F, Jaffe D, Gassó S, Gill T, Laulainen NS, Lu F, Reheis MC, Chun Y, Westphal D, Holben BN, Gueymard C, McKendry I, Kuring N, Feldman GC, McClain C, Frouin RJ, Merrill J, DuBois D, Vignola F, Murayama T, Nickovic S, Wilson WE, Sassen K, Sugimoto N, Malm WC (2001) Asian dust events of April 1998. *J Geophys Res* 106(D16):18317–18330, [10.1029/2000JD900788](https://doi.org/10.1029/2000JD900788)
- In H-J, Park S-U (2002) A simulation of long-range transport of Yellow Sand observed in April 1998 in Korea. *Atmos Environ* 36:4173–4187
- In H-J, Park S-U (2003) The soil particle size-dependent emission parameterization for an Asian dust (Yellow Sand) observed in Korea on April 2002. *Atmos Environ* 37:4625–4636
- Kerr JT, Ostrovsky M (2003) From space to species: ecological applications for remote sensing. *Trends Ecol Evo* 18:299–305
- Lee E-H, Park S-U (2005) A numerical simulation of an Asian dust (Hwangsa) event observed in Korea on March 10–12, 2004 using the modified ADAM model. *Adv Geosci* 5:67–76
- Lu L, Li X, Huang CL, Ma MG, Che T, Bogaert J, Veroustarate F, Dong QH, Ceulemans R (2005) Investigating the relations between ground-measured LAI and vegetation indices in an alpine meadow, north-west China. *Int J Rem Sens* 26(20):4471–4484
- Martimorena B, Bergametti G (1995) Modeling the atmospheric dust cycle: 1 Design of a soil-derived dust emission scheme. *J Geophys Res* 100:16515–16430
- Park S-U, In H-J (2003) Parameterization of dust emission for the simulation of the Yellow Sand (Asian dust) observed in March 2002 in Korea. *J Geophys Res* 108, (D19) 4618, doi:[10.1029/2003JD00348](https://doi.org/10.1029/2003JD00348).
- Park S-U, Lee E-H (2004) Parameterization of Asian dust (Hwangsa) particle-size distributions for use in dust emission model. *Atmos Environ* 38:2155–2162
- Park S-U, Lee E-H (2005) A numerical simulation of an Asian dust event observed in Korea on 20–22 April 2005 with the ADAM2 model. *Proceedings of 11th International Joint Seminar on Regional Deposition Processes in the Atmosphere*, November 23–25 2005. Jeju, Korea
- Pettorelli N, Vik JO, Mysterud A, Gaillard JM, Tucker CJ, Stenseth NC (2005) Using the satellite-derived NDVI to assess ecological responses to environmental change. *Trends Ecol Evo* 20:503–510
- Telesca L, Lasaponara R (2006) Vegetation patterns in burned and unburned areas investigated by using the detrended fluctuation analysis. *Physica A* 368:531–535
- Thaim AK (2003) The causes and spatial pattern of land degradation risk in southern Mauritania using multitemporal AVHRR-NDVI imagery and field data. *Land Degrad Dev* 14:133–142
- Tucker CJ, Dregne HE, Newcomb WW (1991) Expansion and contraction of the Sahara Desert between 1980 and 1990. *Science* 253:299–301
- Wang Q, Adiku S, Tenhunen J, Granier A (2005) On the relationship of NDVI with leaf area index in a deciduous forest site. *Rem Sens Environ* 94:244–255
- Weiss JL, Gutzler DS, Coonrod JEA, Dahm CN (2004) Long-term vegetation monitoring with NDVI in a diverse semi-arid setting, central New Mexico. *J Arid Environ* 58:249–272
- Westphal DL, Toon OB, Carlson TN (1987) A two-dimensional investigation of the dynamics and microphysics of Saharan dust storms. *J Geophys Res* 92:3027–3049
- Wu B, Liu C (2000) Crop growth monitor system with coupling of AVHRR and VGT Data, *Vegetation 2000*. Lake Maggiore, Italy
- Yi H, Yaokun X (1986) The soil atlas of China, compiled by the Institute of Soil Science. Academia Sinica, Chinese, English
- Zou XK, Zhai PM (2004) Relationship between vegetation coverage and spring dust storms over Northern China. *J Geophys Res* 109: D03104. doi:[10.1029/2003JD003913](https://doi.org/10.1029/2003JD003913)